Available online at www.sciencedirect.com
ScienceDirect
Trans. Nonferrous Met. Soc. China 26(2016) 74−84
Transactions of Nonferrous Metals Society of China
www.tnmsc.cn

Mechanical and ballistic properties of powder metal 7039 aluminium alloy joined by friction stir welding

Mehmet ERDEM[1], Hanifi CINICI[2], Ugur GOKMEN[3], Halil KARAKOC[4], Mehmet TURKER[2]

1. Mechanical Engineering Department, Inonu University, Malatya 44280, Turkey;
2. Metallurgy and Materials Engineering Department, Technology Faculty, Gazi University, Ankara 06560, Turkey;
3. Technical Science Vocational School, Gazi University, Ostim, Ankara 06374, Turkey;
4. Ankara Chamber of Industry 1st Organized Industrial Zone Vocational School, Hacettepe University, Ankara 06935, Turkey

Received 18 March 2015; accepted 28 September 2015

Abstract: 7039 Al alloy plates which were used as armor materials were produced by powder metallurgy method. The prepared mixed powders were pressed and plated by extrusion process. These plates, after being subjected to T6 heat treatment, were joined double-sided by friction stir welding method. Microstructure and microhardness of the welded plate were investigated. It was determined that the finest grain structure and the lowest hardness value occurred in the stir zone as 2−6 μm and HV 80.9, respectively. In order to determine the ballistic properties of welded plates, 7.62 mm armor piercing projectiles were shot to the base metal (BM), heat affected zone (HAZ), and thermomechanically affected zone+stir zone (TMAZ+SZ). Ballistic limits (v_{50}) of these zones were determined. The ballistic limits of the BM, TMAZ+SZ, and HAZ of the plate were approximately 14.7%, 15.3%, and 17.9% lower than that of the standard plate at the same thickness, respectively. It was determined that the armor piercing projectiles created petaling and ductile hole enlargement failure types at the armor plate. Ballistic and mechanical results can be enhanced by hot−cold rolling mills after extrusion and particle reinforcement.

Key words: powder metal 7039 Al alloy; ballistic limit; microstructure; mechanical properties

1 Introduction

Characteristics like ballistic performance, lightness, high mobility and weldability are significantly important for the materials and vehicles used in the defense systems. The type and the mechanical properties of armor materials affect the ballistic performance. Density of the armor materials specifies the mobility of vehicles whereas weldability of armor materials determines the watertightness especially in the amphibian operations [1]. Therefore, studies to increase the ballistic performance of light materials have increased. 7xxx series aluminium alloys can be hardened by aging heat treatment and particle sizes can be controlled by recrystallization. Especially, 7039 aluminium alloys, due to their high strength and energy absorption capacity, have a distinctive significance. These materials are being used in the combat vehicles as armor material [2−5].

In the welded joints, suitable joint design, welding heat efficiency, width of heat affected zone, hardness and microstructure variations are the principal causes which affect the mechanical and ballistic strengths. The ideal selection of these parameters plays a determinant role in the protection of mechanical and ballistic properties of welded materials. In some studies [6,7], when the hardnesses of Al base armor plates were increased by heat treatment, ballistic performances of armor plate increased and a decrease of approximately 25% was observed in the armor mass. JENA et al [8] specified that in 7017 Al alloy plates, as the thickness increased, the ballistic performance against the 7.62 mm projectiles of 830 m/s impact velocity increased. ERDEM and TÜRKER [1] joined 7039 aluminium alloy armor plates (having MIL-DTL-46063H standard) of 38 mm thickness by metal inert gas (MIG) welding with multiple passes. They made shots with 12.7 mm armor-piercing projectiles to the base metal (BM), the heat affected zone (HAZ), and the welding metal (WM). The ballistic limit value v_{50} was determined for these zones.

Corresponding author: Mehmet ERDEM; Tel: +90-422-3774783; Fax: +90-422-3410046; E-mail: mehmet.erdem@inonu.edu.tr
DOI: 10.1016/S1003-6326(16)64090-6

They specified that the occurrence of the residual strain and microstructure variations caused ballistic strength losses in the WM and HAZ. MADHUSUDHAN REDDY et al [9] observed that the grain size was changed depending on heat input in the steel plates which were joined by different welding methods. They also concluded that the ballistic performance changed depending on the impact angle. SADANADAN and HETHERINGTON [10] applied ballistic performance tests to armors of various angles with balls and 7.62 mm armor-piercing projectiles and specified that as the impact angle increased, the ballistic limit v_{50} increased.

When the materials are joined by fusion welding methods, they are subjected to intensive heat input. If this heat input increases, the width of the HAZ increases and the grain structure changes. These changes in the microstructure of the material adversely affect the ballistic performance and the mechanical properties [9,11,12]. The heat input in the friction stir welding (FSW) is less compared with that of fusion welding methods [13,14]. The heat input can be controlled by decreasing the tool rotation velocity and increasing the feed rate or external water cooling. By this way, the hardness and strength values can also be increased [15].

In this study, the powder metal 7039 Al alloy plates were joined by FSW. The microstructure and microhardness examinations were made on the samples taken from welding cross section. The ballistic limits v_{50} for the BM, HAZ and thermomechanical affected zone (TMAZ)+stirred zone (SZ) of the welded plate were calculated. The obtained results were compared with each other and with the ballistic limit v_{50} in the MIL-DTL-46063H standard of the 7039 Al alloy plate at the same thickness [16]. The ballistic limits v_{50} of powder metal 7039 Al alloy welded plates were not previously studied.

2 Experimental

7039 Al alloy is an Al−Zn−Mg alloy which gains strength from precipitation hardening. Microstructure of as-received 7039 Al alloy has $MgZn_2$ precipitates which are embedded in the matrix of α aluminum grains [17]. The MIL-DTL-46063H-7039 Al alloy (its chemical composition and the particle size and purity of powders are given in Tables 1 and 2, respectively) was produced from powder metal. The mixed powders were pressed at 250 MPa pressure, extruded at 500 °C so that plates of 22 mm × 100 mm × 300 mm were obtained. The defects which occurred on the surface of the plates during fabrication were machined by milling machine and the thickness of the plates was reduced to 20 mm. These plates were kept at 450 °C for 2 h for T6 heat treatment and then water cooled. Later, they were subjected to artificial aging at 120 °C for 24 h. T6 temper condition includes quenching and artificial aging. Pre- and post-aging tensile strength results of the fabricated plates are given in Table 3. The aged plates were joined double-sided by FSW at 1400 r/min and 50 mm/min feed rate at room temperature. The stirring tip was made of HSS steel and its shoulder design which is shown in Fig. 1 was used. The butted plates were clamped on a

Table 1 Chemical composition of Al armor plate MIL-DTL-46063H-7039 (mass fraction, %)

Zn	Mg	Mn	Cu	Fe
3.5−4.5	2.3−3.3	0.1−0.4	0.1	0.4
Si	Cr	Ti	Others	Al
0.3	0.15−0.25	0.1	0.15	Bal.

Table 2 Particle size and purity of powders

Element	Purity/%	Particle size/μm
Al	99.99	<150
Zn	99.9	<50
Mg	99	<100
Mn	99	<50
Cu	97	<120
Fe	99	<150
Si	99.9	<10
Cr	99.9	<100
Ti	98.98	<100

Table 3 Tensile strength results of samples

Sample	Thickness/mm	Tensile strength/MPa	Yield strength/MPa	Elongation/%
MIL-DTL-46063 H (unwelded)	<38	413.6	351.6	9
	>38	393	331	8
Powder metal (unaged)	5	278	228	11.2
Powder metal (aged)	5	317	268	9.8

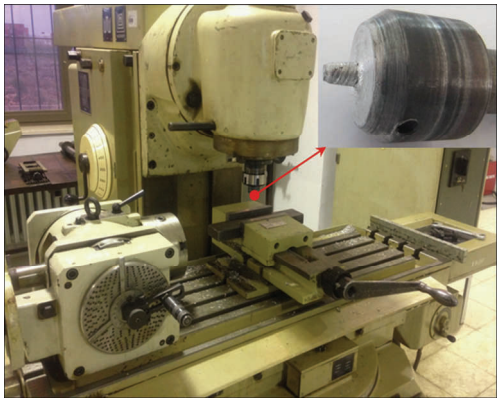

Fig. 1 Universal milling machine and stirring tip

steel backing plate. Welding was carried out via the universal milling machine (Fig. 1). The stirrer tip was rotated in clockwise in welding.

In the experiments, the ballistic test methodology was referenced from MILSTD-662 F standard [18]. Parameters of ballistic experiment are given in Table 4. The v_{50} limit is the most significant factor for determining the ballistic limit value of the armor plate. v_{50} limit is defined as the limit for 50% penetration or non-penetration probability of the armor plate. To determine this limit, at least four shots are made on the plate. Among these four shots, two of them must be of penetrating plate values and the other two must be of non-penetrating values. The velocity value which is gained by subtracting the non-penetrating projectile velocity value from the penetrating projectile velocity value must be 18 m/s. The arithmetic average of these impact velocities gives the ballistic limit value v_{50} [18].

The FSW process changed the grain size and hardness of the powder metal 7039 Al alloy plates in the HAZ and TMAZ+SZ areas. In order to determine the effect of these changes on the ballistic limit v_{50}, the BM, HAZ and TMAZ+SZ areas were marked on the plate. If the ballistic limit v_{50} of the plates is thinner than 20 mm of the MIL-DTL-46063H standard, the ballistic limit is estimated at 30° oblique. Consequently, the welded target plate was fixed at 30° oblique during the ballistic experiment. The shots were made with 7.62 mm armor piercing projectiles to the marked areas on the plate by laser pointer. The velocities of the projectiles were controlled by the decrease or the increase of the gunpowder amount. The ballistic limit values v_{50} for each of the areas were estimated in the end of the ballistic experiment. These values were compared with each other, and with the ballistic limit value v_{50} of the 7039 Al alloy plate (MIL-DTL-46063H).

The FSW samples were cross-sectioned perpendicular to the welding direction, polished, and then etched with Keller solution. For the purpose of determining the changing characteristics at the welding section, microhardness and microstructure examinations were carried out by using 100 g load at the Shimadzu HMV-G and optical microscope LAICA DM4000M, respectively. The microstructural characterization was performed with Leo EVO−40 VPX scanning electron microscope (SEM) with attached Bruker X flash detector 4010 energy dispersive X-ray spectroscope unit (EDX).

3 Results and discussion

3.1 Microstructure

The microstructures of welding section zones are given in Fig. 2. It was observed that the grains elongated towards the extrusion direction in the BM microstructure (Fig. 2(a)). These grains were approximately 50 μm in length and 8 μm in width. The fine equiaxed grains were observed among these elongated grains in some zones. It is thought that the equiaxed grains occurred with recrystallization which took place during hot extrusion. The structure of elongated grains was disordered and became coarse in the HAZ (Fig. 2(b)). The significant factor for the change of structure grain is the friction heat of the stirring tip. The thermomechanical effect of the stirring tip directed the grains to the direction of the rotation (Fig. 2(c)). The aspect ratio of the directed grains increased. The sizes of grains in the SZ are uniform compared with other zones such as the BM, HAZ, and TMAZ (Fig. 2(d)). The joining defect was not observed in the SZ. Therefore, the Al plates were successfully joined by the FSW. The crack in cross-section is the fracture crack which came into existence with the impact effect of armor projectile. The field of plastic deformation increased and size of the SZ enlarged due to the stirring double side. The SEM images of welded plate cross-section were given in Figs. 3(a)−(c). The grains in the SZ which were caused by dynamic recrystallization were in 2−6 μm size range.

In the microstructure of the welded plate, the existence of the four different zones (SZ, TMAZ, HAZ, and BM) was explicitly specified. The grains in the SZ were finer than those in other zones. The similar finer grains were obtained in the SZ of Cu and brass materials [19]. SHARMA et al [20] joined the 7039 Al alloy extruded plates of 5 mm thickness by the FSW. They used 75 mm/min traverse velocity and 635 r/min rotation velocity in the FSW. They specified that the weld nugget zone had finer grain structure than the BM, TMAZ and HAZ. They observed that the fine microstructure zone decreased when moved away from the weld center and the grains in the TMAZ bent and flattened due to tool stirring effect. They stated that HAZ had coarser grain structure compared with the BM. In another study, SHARMA et al [21] joined the 7039 Al alloy plates with thickness of 5 mm by the FSW at different rotation rates and traverse velocities. They observed that the traverse velocities and rotation rates caused intensive plastic deformation and high temperature in the FSW. All weld nuggets were dynamic recrystallized by intensive plastic deformation and high temperature. These zones were of refined equiaxed grain structure. The coarse grain in the BM changed to refined and equiaxed grain structure in the nugget zone. The nugget zone was surrounded by the TMAZ and the Al grains were non-uniformly deformed by tool during the stirring. XU et al [22] joined the 2219-T62 Al alloy plates of thickness 12 mm by the FSW at different rotation rates and traverse velocities. They observed that the grain structure of the BM consisted of large elongated pancake shaped grains. The

Table 4 Ballistic test parameters

Barrel type	Bullet type	Gunpowder	Core mass/g	Oblique/(°)	Bullet diameter/cm	Temperature/°C	Pressure/kPa
OBERMAYER cal.0.30, 76 cm	7.62 mm APM2	MKE	163.5	30	0.76	15	928

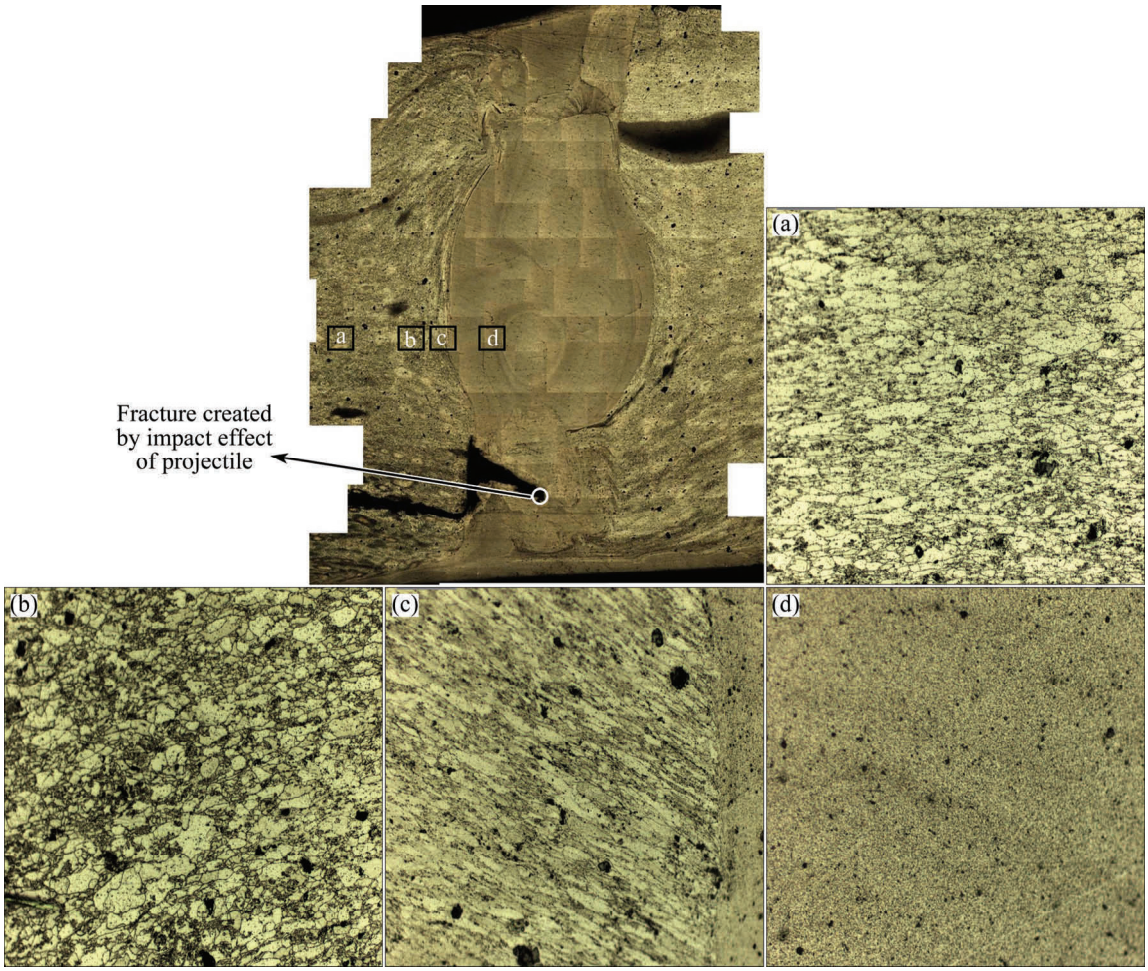

Fig. 2 Section view and microstructure of plate welded by FSW: (a) BM; (b) HAZ; (c) TMAZ; (d) SZ

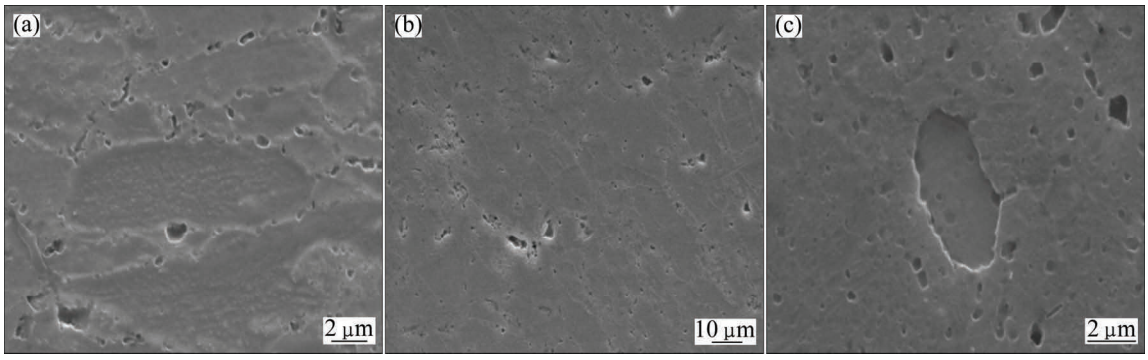

Fig. 3 SEM images of microstructure: (a) BM; (b) TMAZ; (c) SZ

stirred zone consisted of equiaxial grains with dynamic recrystallization. The size of these grains spanned from 5.5 to 3.5 μm. They stated that highly deformed and elongated grains were seen in the TMAZ because of stirring and plastic flow. The grains in the HAZ grew gradually large because of heat. İPEKOĞLU et al [23] investigated the effect of two temper conditions (AA7075-O and AA7075-T6) on mechanical properties and microstructure of welded plate. As a result, they concluded that the change of plastic deformation amount

affected the recrystallized grains.

In the EDAX analysis (Fig. 4), the percentage ratios of matrix to main alloy elements were determined. In Fig. 5, the result of elemental mapping analysis showed that distribution of these elements was uniform in the matrix.

3.2 Microhardness

Figure 6 shows the center cross section of the welded plate. Figure 7 gives microhardness results of perpendicular section. The hardness value of BM was approximately HV 107. In the hardness taken along with the welding center, the highest hardness value was HV 129 in the TMAZ and in the retreated side, whereas the lowest hardness value was HV 80.9 in the stirred zone. The lowest hardness value in the HAZ was HV 92.2 in the advanced side. While the hardness curve taken from the section center was symmetrical in the stirred zone, it was asymmetrical in the TMAZ and the HAZ. In the stirred zone, the hardness was at the lowest value. It is thought that the thermal cycle of the FSW in this area causes re-dissolution and coarsening of second phase precipitates, and for this reason, the hardness decreased. On the other hand, the hardness increased in the TMAZ. It is also estimated that the redissolution and coarsening of second phase precipitates in this area were less than the stirred zone. Besides, the grains were

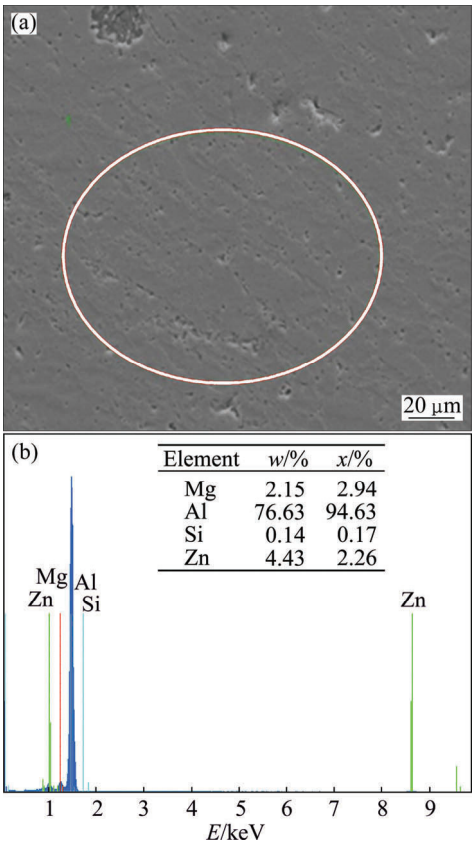

Fig. 4 SEM image (a) and EDAX results (b) of BM

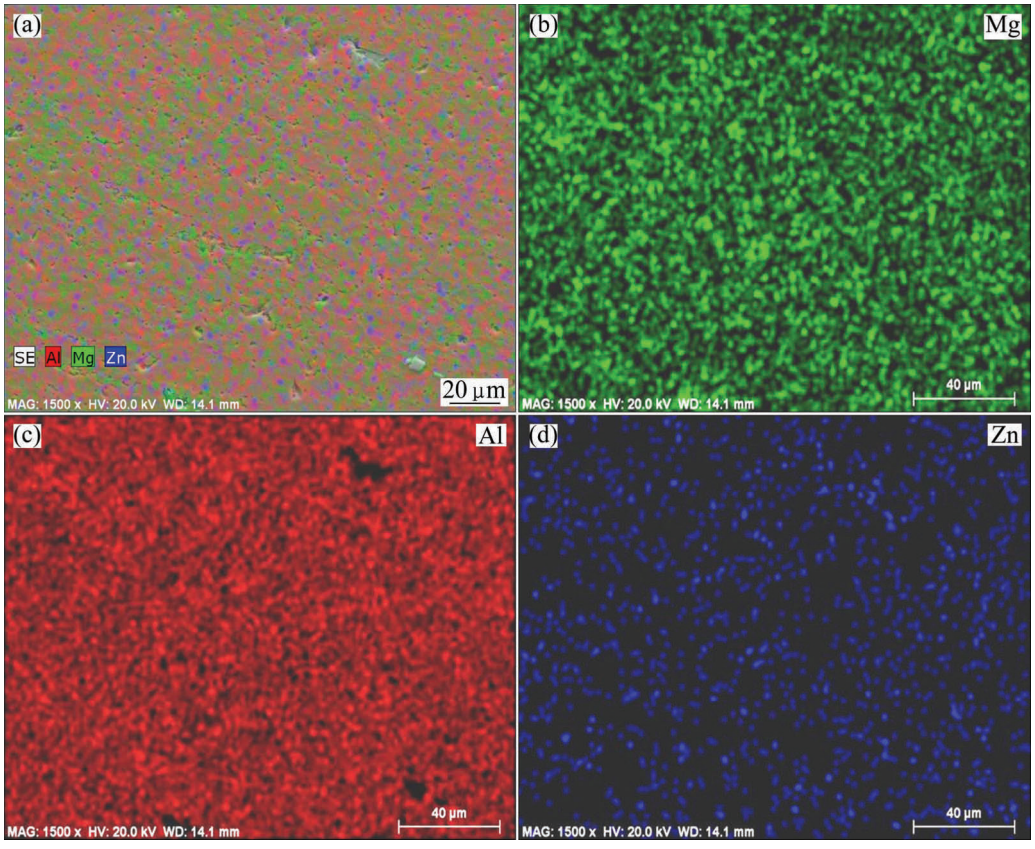

Fig. 5 SEM image (a) and elemental mapping results (b, c, d) of BM

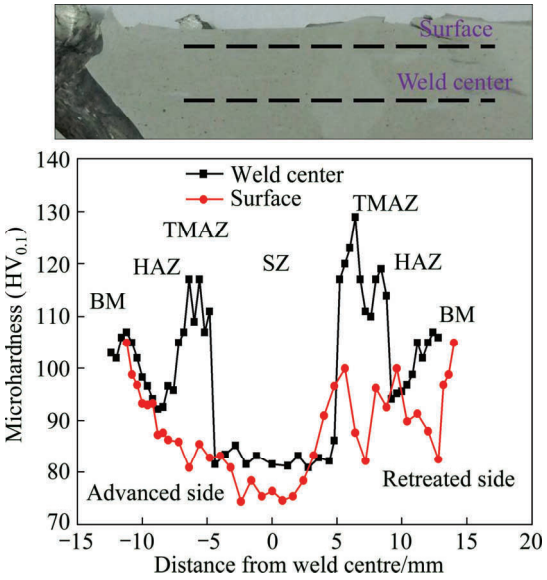

Fig. 6 Microhardness values of different zones

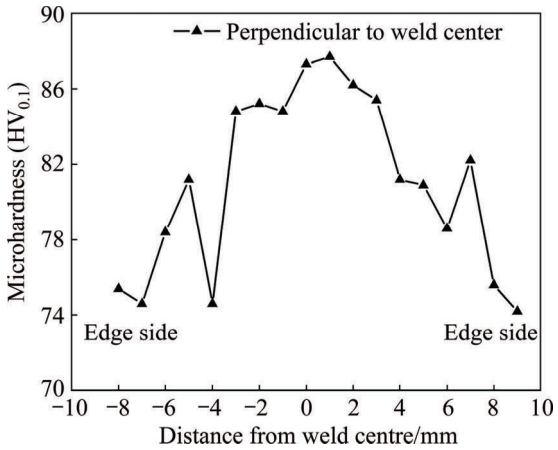

Fig. 7 Microhardness values of SZ

directed with thermomechanical effect in the direction of tool rotation and as a result the plastic strains were created in the TMAZ. These strains increased the hardness in this area. The decrease of hardness in the HAZ is the natural result of thermal cycle of the FSW in the aged Al alloys [22].

The hardness values of the BM, HAZ, TMAZ, and SZ are approximately HV 107, HV 92.2, HV 129, and HV 80.9, respectively. The results obtained in this study are consistent with the literature. GUO et al [24] joined the T6 temper AA6061 and AA7075 alloys by the FSW and stated that the microhardness decreased in the welding zone. Because the thermal cycle of the FSW caused coarsening and re-dissolution of precipitates, the hardness decreased. The lowest hardness was in the HAZ of the AA6061 Al alloy. On the same subject, LIU and MA [25] specified that in the precipitation hardened Al alloys, the FSW created a softened area in the heat affected zone and the lowest hardness value was in the HAZ. They added that during the thermal cycle of the FSW, most of the precipitates re-dissoluted and coarsened, and this decreased the hardness. SHARMA et al [21] joined the 7039 Al alloy by the FSW under different welding conditions. They determined that as the heat input to welding zone decreased, microhardness and tensile properties increased. In all of the joints, the hardness was maximum in the TMAZ of the retreating side and the hardness curve was asymmetrical compared with welding center. The high temperature strengthening on the advancing side caused more coarsening and re-dissolution of precipitates which led to lower hardness. The TMAZ average microhardness was higher than those of the nugget zone and the HAZ. They claimed that during FSW, solid atom concentration increased for the suitable precipitation hardening and solid solution hardening due to natural aging in the TMAZ (exposed to higher temperature than the HAZ), and for this reason, hardness in the TMAZ increased. The hardness decrease in the HAZ was due to the re-dissolution of second phase precipitates. Additionally, they stated that the forging hardening effect on the TMAZ was higher than that on the weld nugget and the HAZ, and this could contribute to hardness improvement in another study. SHARMA et al [20] specified that the heat treatments after welding radically affected the microhardness distribution. After joining by FSW, they found that the hardnesses in WNZ, HAZ and BM were HV 115.3, HV 107.6 and HV 135, respectively. It was stated that the precipitation hardened the Al alloys, a soft zone was created around the weld center, and this softened zone resulted from re-dissolution and coarsening of the precipitations during the thermal cycle of the FSW [26]. GRUJICIC et al [27] stated that HAZ, TMAZ and SZ sections of the material were exposed to high temperature during FSW. Therefore, over-aging occurred on the precipitates of these sections in age-hardenable material. This over-aging resulted in loss of strength/hardness in these areas. In this study, hardness values of the HAZ and SZ decreased. GRUJICIC et al [28] expressed that the SZ of nonage-hardenable alloys (AA5083-H131) tended to dynamically recrystallize based on high weld temperature and heavily plastically deformation during the FSW. The strength/hardness of the dynamically recrystallized zone lessened relative to the base metal. The strength and ductility of nonage-hardenable alloy were mainly controlled by the grain size and strain hardening [29].

The friction heat was raised more on the contacted regions of the shoulder of the stirring tip during the FSW. The plate surface was exposed to more heat input compared with its center. Therefore, the hardness value taken from the area close to surface was less than the hardness value taken from the welding center. In the

areas where the heat input was high, the hardness decreased. The hardness values measured as perpendicular to the SZ decreased in the side areas where the heat input was high and increased in the center where the heat was low.

3.3 Ballistic properties

The 7039 Al alloys plates were fabricated by powder metallurgy method and these plates were welded by the FSW. Ballistic properties of the welded plate were calculated by the shootings to the BM, HAZ and TMAZ+SZ. The results of these shooting are given in Table 5. In this table, the velocity average is the arithmetic average of projectile velocities. This average was measured by the first and second detectors. In the calculation of ballistic limits v_{50} of these zones, the marked velocity values in Table 5 were used. All of the ballistic results v_{50} which were separately calculated for each zones and standard plate (MIL-DTL-46063H) are given in Table 6.

Table 5 Ballistic experiment results of BM, HAZ and TMAZ+SZ

Material	Shot No.	Powder mass/g	Velocity/(m·s^{-1})			Results
			Avg.	loss	Striking	
BM	1	1.80	548	2	546	CP
	2	1.70	520	2	518*	CP
	3	1.69	513	2	511*	CP
	4	1.68	508	2	506*	PP
	5	1.67	505	2	503*	PP
	6	1.65	488	2	486	PP
HAZ	1	1.80	545	2	543	CP
	2	1.70	509	2	507*	CP
	3	1.69	515	2	513*	CP
	4	1.67	499	2	497*	PP
	5	1.68	506	2	504*	PP
TMAZ+SZ	1	1.68	507	2	505	CP
	2	1.67	500	2	498*	CP
	3	1.66	493	2	491*	CP
	4	1.64	485	2	483*	PP
	5	1.65	491	2	489*	PP

PP: Partial penetration; CP: Complete penetration

In this study, the ballistic limits v_{50} were determined separately for all of the zones. The microstructure and microhardness results of all of the zones were compared with each other. The microstructure and microhardness results were discussed in Sections 3.1 and 3.2, respectively. The BM microstructure consisted mainly of extrusion directed elongated grains and equiaxed finer grains. The hardness of this zone and the ballistic limit

Table 6 MIL-DTL-46063H standard and obtained v_{50} ballistic limits values

Material	v_{50} ballistic limit/(m·s^{-1})	According to standard value loss of velocity/%
Standard	597.1	
BM	509.5	14.7
HAZ	490.3	17.9
TMAZ+SZ	505.5	15.3

v_{50} were determined as HV 107 and 509.5 m/s, respectively. The ballistic limit v_{50} of the BM decreased by 14.7% compared with the standard ballistic limit v_{50} (MIL-DTL-46063H). The grains were refined because of recrystallization in the SZ. The hardness decreased due to redissolving and coarsening of second phase precipitation in this zone. The stirring tip caused thermomechanic effect in the TMAZ. This effect directed the grains towards the rotation route. The plastic strains were generated by the thermomechanic effect in this zone and these strains increased the hardness. Although the SZ had the lowest hardness, the TMAZ had the highest hardness. Therefore, the ballistic limit v_{50} of the TMAZ+SZ slightly decreased (505.5 m/s). This value decreased by 15.3% compared with the standard ballistic limit value v_{50} (MIL-DTL-46063H). In the HAZ, the structure of the extrusion directed elongated grains disordered and coarsened, and the hardness of the HAZ decreased because of the friction heat of the stirring tip. Therefore, the v_{50} ballistic limit of the HAZ was at the lowest value (490.3 m/s). This value decreased by 17.9% compared with the standard ballistic limit value v_{50} (MIL-DTL-46063H). The highest ballistic limit value v_{50} was determined on the BM. The percentages of ballistic limits v_{50} of the TMAZ+SZ and the HAZ to that of the BM were 99.13% and 96.36%, respectively.

After the shootings, there were obvious deformation forms on the surface of the different zones of the target plate. The images of deformation are given in Fig. 8. The ballistic limits v_{50} of each zone had been calculated by two projectile velocities which had completely penetrated to the armor plate. In the zones, the deformation was caused by the projectiles. The images (Fig. 8) belong to these projectiles. The hardness of the zones changed and this situation affected the deformation forms in the exit and entry of the penetration channel. In generally, as the projectile impact velocity increased, the crater formation increased due to impact effect in all of the three zones. In Fig. 8(a), the front and back images of BM areas are given. In the front image, the impact effect created a crater and a crater convolution towards outside. The fractures occurred around this crater with the impact effect. In Fig. 8(b), front and back images of the TMAZ+SZ are given. In the front images of this zone,

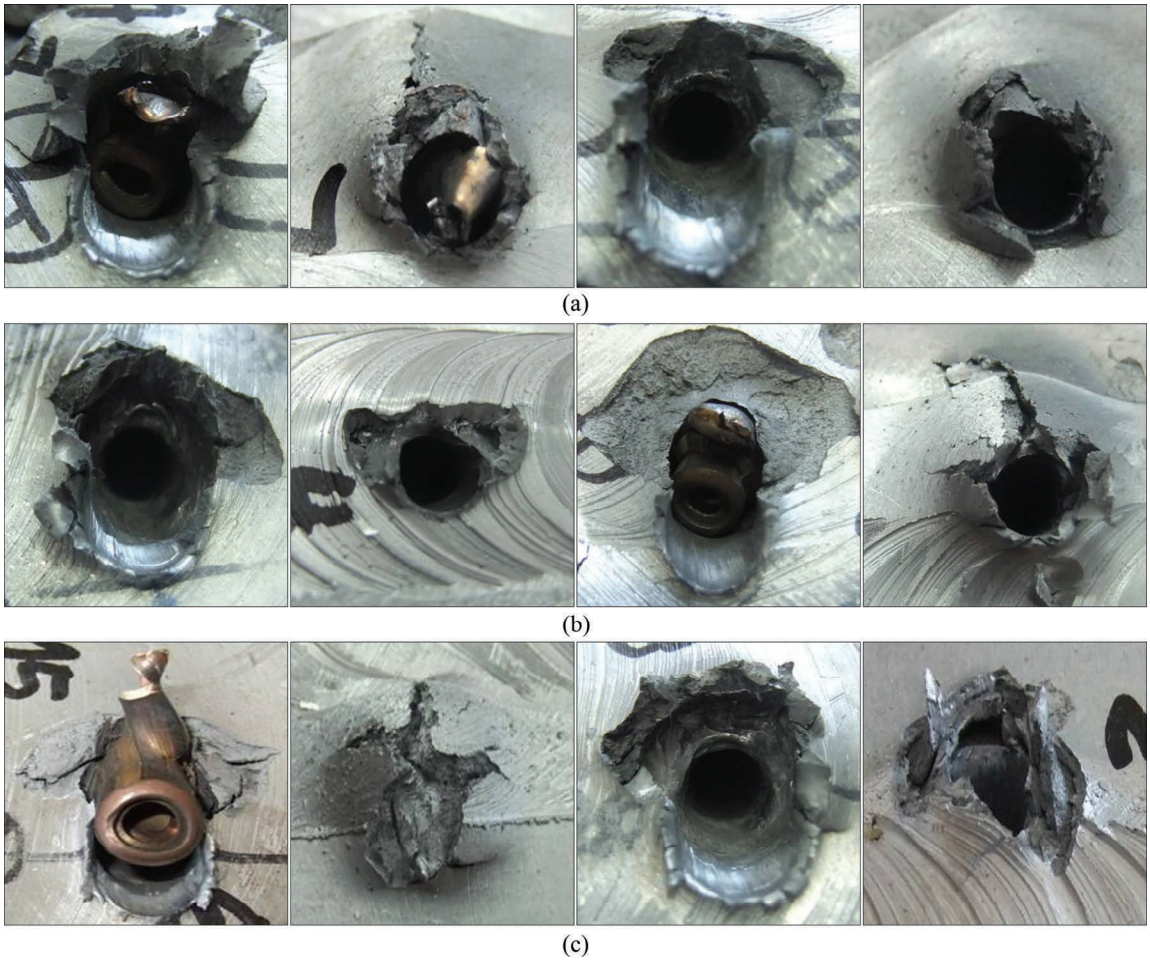

Fig. 8 Post-ballistic test, front and back images of plate surface: (a) BM; (b) TMAZ+SZ; (c) HAZ

crater convolution exhibited a more ductile plastic behavior with respect to base metal. The surface fractures increased due to the decrease in hardness in the SZ and the surface zone of the TMAZ. In Fig. 8(c), front and back images of the HAZ are given. It was shown that the convolutions on the impact surface resembled in the TMAZ+SZ. The surface fractures also occurred in this zone.

The ballistic limits v_{50} of the BM, TMAZ+SZ, and HAZ of the plate were approximately 14.7%, 15.3%, and 17.9% lower than that of the standard plate at same the thickness (MIL-DTL-46063H), respectively. In this study, the obtained results are coherent with the literature. SULLIVAN et al [30] determined that there was a great loss of hardness in the HAZ due to overaging in the ballistic limit v_{50} tests of the 7010 Al alloy plate. In this area, the ballistic limits v_{50} decreased by 20% and 10% for armor piercing projectiles and fragmented simulated projectiles, respectively. MONDAL et al [31] specified that the hardness and strength of the unaged 7055 Al cast alloy target were higher compared with the overaged target and at the same time its ballistic penetration resistance was much better. HOLMEN et al [32] applied T6 temper to the AA6070 alloy plate of 20 mm thickness, and specified that the ballistic impact resistance of the plate increased. Plate thickness and projectile impact angle are the parameters affecting the ballistic limit v_{50}. GU et al [33] applied T9I6 temper to the AA2519 alloy plate of 30 mm thickness, and determined that the ballistic limit v_{50} of this plate was 715 m/s. JENA et al [8] determined that the 27−28 and 30 mm thickness of the 7017 Al plates successfully stopped a projectile of 830 m/s impact velocity whereas the 26 mm thickness of the Al plate was penetrated. SADANADAN and HETHERINGTON [10] used 7.62 mm armor piercing projectiles with zero impact angle in their ballistic performance tests. They specified the ballistic limit v_{50} of alumina−Al armor as 700 m/s and the ballistic limit v_{50} of alumina−steel armor as 634 m/s. In the tests made with balls, they obtained the ballistic limit of alumina−Al armor as 800 m/s and the ballistic limit v_{50} of alumina−steel armor as 631 m/s. WANG et al [34] applied two heat treatments to the Ti-55531 alloy plate of 8 mm thickness. They attained high-strength and high-toughness plates. They determined that the v_{50} values of these plates were 330 m/s and 390 m/s, respectively. KARAMIŞ et al [35] carried out a ballistic test on the metal matrix composite. The ductile hole

surface on the composite was formed by the high impact velocity and friction heat of the projectile when the projectile was entering. On the other hand, there became a coarse hole when the projectile was exiting depending on its low velocity and friction.

Figure 9 shows the deformation of the armor piercing projectile (HRC 63.3) which was shot to the SZ. The hardness of the TMAZ in the center of the plate was higher compared with that of the TMAZ which was close to the surface. For this reason, the projectile followed a curved route (even if in minor amount) in the area of the higher hardness. At the tip of the projectiles, no visible deformation was observed. As it is seen in the detailed picture of the area close to the projectile tip, the effect of impact multiplied the shear bands and these bands caused the beginning of the fracture cracks.

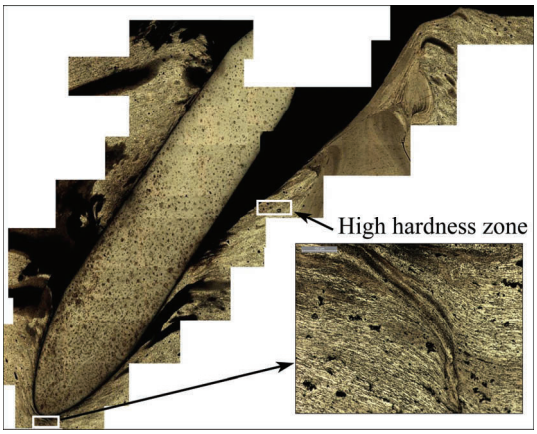

Fig. 9 Projectile deformation in TMAZ+SZ

The penetration channels occurred in different zones depending on the armor piercing projectiles. These forms on the channels are shown in Fig. 10. The lengths of penetration channels increased on the grounds of the impact angle which was 30°. In all zones, while the intake of penetration channel was wide, the exit of penetration channel was narrow. The hardness and projectile velocity affected the exit and the intake forms of penetration channel. The friction forces are intensive because of high projectile velocity in the intake of penetration channel. The friction heat increases and the penetration channel gets widened due to these forces. The projectile velocity decreases, when crossing the penetration channel. The friction force and heat decrease in the exit of penetration channel [35]. Therefore, the exit of penetration channel was not enlarged by the projectile. It is shown in Figs. 10(a), (b) and (c) that the penetration channels were formed by different velocities of the projectiles in the BM, HAZ, and TMAZ+SZ, respectively. The width of the penetration channel in the HAZ was larger than that in the BM. It is thought that the situation was caused by the decrease in hardness of the HAZ. The width of penetration channel in the SZ was larger compared with that in the HAZ, depending on the decrease in hardness of the SZ.

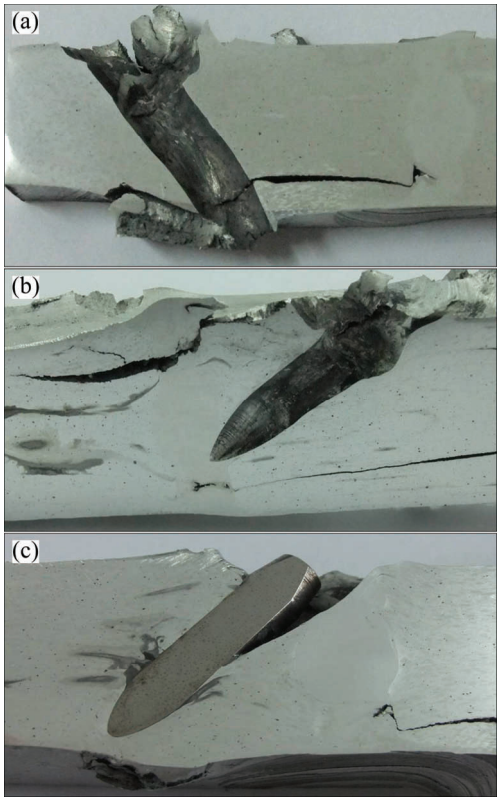

Fig. 10 Macro images of deformation created along plate section of armour piercing projectiles: (a) BM; (b) HAZ; (c) TMAZ+SZ

In this study, the armor piercing projectiles create front/back face petaling and ductile hole enlargement failure types at the plate. These failure types showed similarity with those determined by GRUJICIC et al [36]. While the front-face petaling failure mechanism occurs under most ballistic-impact loading conditions, the extent of back face petaling is affected by the target-material hardness. The hardness and ductility of the material have an effect on this type of failure. Types of the ductile hole enlargement failure mechanism are affected by the projectile shape, size, velocity, and the target thickness. It is generally observed in the case of thicker targets impacted by ogive-shaped projectiles. This failure type is greatly affected by the hardness of the target material [36].

4 Conclusions

1) Because of the dynamic recrystallization, the grain structure in the SZ was finer (2−6 μm) compared with that in other zones. It was observed that the grains in the TMAZ were directed towards tool rotation route

depending on thermomechanical effect of the stirring tip. The width of the directed grains decreased. The grain structure in the HAZ became coarser (even if in minor amount). It was dominantly determined that the grain structure elongated (about 50 μm) towards the direction of extrusion in the BM. The microstructure changed with the stirring effect and consisted of four different zones (BM, HAZ, TMAZ and SZ).

2) The highest hardness value was in the retreated side of TMAZ being HV 129 and the lowest hardness value was in the stirring zone as HV 80.9. The lowest hardness value in the HAZ was HV 92.2. The BM hardness value was about HV 107. During the FSW, since the tool shoulder of the stirring tip touched a large area and the heat input affected a large area as well, the hardness of the areas close to surface decreased. The hardness increased due to lower heat input in the central of the weld section.

3) The ballistic limits v_{50} of the BM, TMAZ+SZ, and HAZ of the plate were approximately 14.75%, 15.3%, and 17.9% lower than that of the standard plate at same thickness (MIL-DTL-46063H), respectively. The ballistic limits v_{50} of the TMAZ+SZ and the HAZ were 0.87 and 3.64% lower than that of the BM, respectively. The ballistic limit v_{50} decrease in these zones was slight compared with that in the BM. Although the hardness of the SZ was the lowest, the ballistic limit v_{50} of this zone was excess compared with that in the HAZ. The reason for that was thought to be the hard TMAZ which surrounded the stirred zone like a jacket. The heat input in the FSW is less than that in the fusion welding methods. Therefore, the ballistic limits v_{50} of these zones decreased. In addition, the hardness decreased as the ballistic limit v_{50} decreased.

4) The exit and intake forms of the penetration channel were affected by the projectile velocity and the hardness. The friction force and heat increased because of high projectile velocity in the entry of the penetration channel. Therefore, the gate of the penetration channel was widened by the projectile. The velocity of the projectile slowed along its passing through the penetration channel and the friction force and heat decreased in the exit of the penetration channel. Besides, the exit of the penetration channel did not become enlarged by the projectile. The width of penetration channel in the HAZ was larger than of the BM. It is thought that this situation was caused by the decrease in hardness of the HAZ. The width of the penetration channel in the SZ was larger compared with that in the HAZ, owing to the hardness decrease in the SZ.

5) Ballistic results can be increased by hot-cold rolling mills after extrusion and particle reinforcement.

Acknowledgement

The authors thank to FNNS for the ballistic tests.

References

[1] ERDEM M, TÜRKER M. Investigation of the ballistic and mechanical properties of the pre and post-welded 7039 aluminum alloy [J]. J Fac Eng Arch Gazi Univ, 2011, 26: 17−26.

[2] DUMONT D, DESCHAMPS A, BRECHET Y. On the relationship between microstructure; strength and toughness in AA7050 Al alloys [J]. Mat Sci Eng A, 2003, 356: 326−336.

[3] LUDTKA G M, LAUGHLIN D E. Influence of microstructure and strength on the fracture mode and toughness of 7xxx aluminium alloys [J]. Metall Trans A, 1982, 13: 411−425.

[4] DIXIT M, MISHRA R S, SANKARAN K K. Structure-property correlations in Al 7050 and Al 7055 high-strength aluminium alloys [J]. Mat Sci Eng A, 2008, 478: 163−172.

[5] ZHAO P J, TSUCHIDA T. Effect of fabrication conditions and Cr, Zr contents on the grain structure of 7075 and 6061 aluminium alloys [J]. Mat Sci Eng A, 2009, 499: 78−82.

[6] DEMIR T, ÜBEYLI M, YILDIRIM R O. Investigation on the ballistic impact behavior of various alloys against 7.62 mm armor piercing projectile [J]. Mater and Des, 2008, 29: 2009−2016.

[7] ÜBEYLI M, YILDIRIM O, ÖGEL B, Investigation on the ballistic behavior of Al_2O_3/Al2024 laminated composites [J]. J Mater Proces Tech, 2008, 196: 356−364.

[8] JENA P K, MISHRA B, KUMAR K S, BHAT B T. An experimental study on the ballistic impact behavior of some metallic armour materials against 7.62 mm deformable projectile [J]. Mater and Des, 2010, 31: 3308−3316.

[9] MADHUSUDHAN REDDY G, MOHANDAS T, PAPUKUTTY K K. Effect of welding process on the ballistic performance of high-strength low-alloy steel weldments [J]. J Mater Proces Tech, 1998, 74: 27−35.

[10] SADANANDAN S, HETHERINGTON J G. Characterization of ceramic/steel and ceramic/aluminium armors subjected to oblique impact [J]. Int J Impact Eng, 1997, 19: 811−819.

[11] MADHUSUDHAN REDDY G, MOHANDAS T. Ballistic performance of high strength low alloy steel weldments [J]. J Mater Proces Tech, 1996, 57: 23−30.

[12] MOHANDAS T, MADHUSUDHAN REDDY G, SATISH KUMAR B. Heat affected zone softening in high strength low alloy steels [J]. J Mater Proces Tech, 1999, 88: 284−294.

[13] MERAN C. The joint properties of brass plates by friction stir welding [J]. Mater and Des, 2006, 27: 719−726.

[14] XIE G M, MA Z Y, GENG L. Development of a fine-grained microstructure and the properties of a nugget zone in friction stir welded pure copper [J]. Scpt Mater, 2007, 57: 73−76.

[15] LIU F C, XIAO B L, WANG K, MA Z Y. Investigation of superplasticity in friction stir processed 2219Al alloy [J]. Mat Sci Eng A, 2010, 527: 4191−4196.

[16] Department of Defense, USA. Aluminum alloy 7039, armor plate: MIL-DTL-46063 H [P]. 1998−09−14.

[17] SHARMA C, DWIVEDI D K, KUMAR P. Effect of welding parameters on microstructure and mechanical properties of friction stir welded joints of AA7039 aluminum alloy [J]. Mater and Des, 2012, 36: 379−390.

[18] Department of Defense Test Method Standard. V50 ballistic test for armor: USA, MIL-STD-662 F [P]. 1997−12−18.

[19] ERDEM M. Investigation of structure and mechanical properties of copper-brass plates joined by friction stir welding [J]. Int J Adv Manuf Technol, 2015, 76: 1583−1592.

[20] SHARMA C, DWIVEDI D K, KUMAR P. Effect of post weld heat treatments on microstructure and mechanical properties of friction stir welded joints of Al−Zn−Mg alloy AA7039 [J]. Mater and Des, 2013, 43: 134−143.
[21] SHARMA C, DWIVEDI D K, KUMAR P. Effect of welding parameters on microstructure and mechanical properties of friction stir welded joints of AA7039 aluminium alloy [J]. Mater and Des, 2012, 36: 379−390.
[22] XU W, LIU J, ZHU H, FU L. Influence of welding parameters and tool pin profile on microstructure and mechanical properties along the thickness in a friction stir welded aluminium alloy [J]. Mater and Des, 2013, 47: 599−606.
[23] İPEKOĞLU G, ERIM S, ÇAM G. Effects of temper condition and post weld heat treatment on the microstructure and mechanical properties of friction stir butt-welded AA7075 Al alloy plates [J]. Int J Adv Manuf Technol, 2014, 70: 201−213.
[24] GUO J F, CHEN H C, SUN C N, BI G, SUN Z, WEI J. Friction stir welding of dissimilar materials between AA6061and AA7075 Al alloys effects of process parameters [J]. Mater and Des, 2014, 56: 185−192.
[25] LIU F C, MA Z Y. Influence of tool dimension and welding parameters on microstructure and mechanical properties of friction-stir-welded 6061-t651 aluminum alloy [J]. Metallurgical and Mater Trans A, 2008, 39: 2378−2388.
[26] MISHRA R S, MA Z Y. Friction stir welding and processing [J]. Mater Sci and Eng R, 2005, 50: 1−78.
[27] GRUJICIC M, ARAKERE G, YALAVARTHY H V, HE T, YEN C F, CHEESEMAN B A. Computational investigation of hardness evolution during friction-stir welding of AA5083 and AA2139 aluminum alloys [J]. J Mat Eng and Perform, 2011, 20: 1097−1108.
[28] GRUJICIC M, ARAKERE G, YALAVARTHY H V, HE T, YEN C F, CHEESEMAN B A. Modeling of AA5083 material-microstructure evolution during butt friction-stir welding [J]. J Mat Eng and Perform, 2010, 19: 672−684.
[29] GRUJICIC M, ARAKERE G, HARIHARAN A, PANDURANGAN B. A concurrent product-development approach for friction-stir welded vehicle-underbody structures [J]. J Mat Eng and Perform, 2012, 21: 437−449.
[30] SULLIVAN A, DERRY C, ROBSON J D, HORSFALL I, PRANGNELL P B. Microstructure simulation and ballistic behavior of weld zones in friction stir welds in high strength aluminum 7xxx plate [J]. Mater Sci and Eng A, 2011, 528: 3409−3422.
[31] MONDAL C, MISHRA B, JENA P K, KUMAR K S, BHAT T B. Effect of heat treatment on the behavior of an AA7055 aluminum alloy during ballistic impact [J]. Int J Impact Eng, 2011, 38: 745−754.
[32] HOLMEN J K, JOHNSEN J, JUPP S, HOPPERSTAD O S, BØRVIK T. Effects of heat treatment on the ballistic properties of AA6070 aluminum alloy [J]. Int J Impact Eng, 2013, 57: 119−133.
[33] GU Gang, YE Ling-ying, JIANG Hai-chun, SUN Da-xiang, ZHANG Pan, ZHANG Xin-min. Effects of T9I6 thermo-mechanical process on microstructure, mechanical properties and ballistic resistance of 2519A aluminum alloy [J]. Transactions of Nonferrous Metals Society of China, 2014, 24(7): 2295−2300.
[34] WANG Yan-ling, HUI Song-xiao, LIU Rui, YE Wen-jun. Evaluation of dynamic performance and ballistic behavior of Ti−5Al−5Mo−5V−3Cr−1Zr alloy [J]. Transactions of Nonferrous Metals Society of China, 2015, 25(2): 429−436.
[35] KARAMIS M B, NAIR F, TAŞDEMIRCI A. Analyses of metallurgical behavior of Al−SiC_p composites after ballistic impacts [J]. Composite Structures, 2004, 64: 219−226.
[36] GRUJICIC M, PANDURANGAN B, ARAKERE A, YEN C F, CHEESEMAN B A. Friction stir weld failure mechanisms in aluminum-armor structures under ballistic impact loading conditions [J]. J Mat Eng and Perform, 2013, 22: 30−40.

粉末冶金 7039 铝合金搅拌摩擦焊接头的力学和弹道性能

Mehmet ERDEM[1], Hanifi CINICI[2], Ugur GOKMEN[3], Halil KARAKOC[4], Mehmet TURKER[2]

1. Mechanical Engineering Department, Inonu University, Malatya 44280, Turkey;
2. Metallurgy and Materials Engineering Department, Technology Faculty, Gazi University, Ankara 06560, Turkey;
3. Technical Science Vocational School, Gazi University, Ostim, Ankara 06374, Turkey;
4. Ankara Chamber of Industry 1st Organized Industrial Zone Vocational School, Hacettepe University, Ankara 06935, Turkey

摘　要：采用粉末冶金法制备装甲用 7039 铝合金板材。原材料粉末经压制后挤压成板材。经 T6 热处理后，采用搅拌摩擦焊对板材进行双面焊接。研究焊接板的显微组织和显微硬度。结果表明，搅拌区的晶粒尺寸最小，硬度最低，分别为 2~6 μm 和 HV 80.9。为研究焊接板的弹道性能，采用 7.62 mm 穿甲弹对基体、热影响区、热力影响区+搅拌区进行射击，获得了这些区域的弹道极限值(v_{50})。基体、热力影响区+搅拌区和热影响区的弹道极限值(v_{50})分别比相同厚度普通板材的降低了 14.7%、15.3%和 17.9%。穿甲弹在装甲板上形成花瓣状和延性孔状失效。经挤压和颗粒增强后，热轧−冷轧可提高板材的弹道和力学性能。

关键词：粉末冶金 7039 铝合金；弹道极限；显微组织；力学性能

(Edited by Yun-bin HE)